An efficient FE analysis for complex low flying air bearing slider designs in hard disk drives: Part II Load/Unload and Shock simulations

Puneet Bhargava and David B. Bogy

Computer Mechanics Laboratory

Department of Mechanical Engineering

University of California at Berkeley

Berkeley, CA 94720

Telephone: (510) 642-4975

Fax: (510) 643-9786

puneet@cml.me.berkeley.edu

April 7, 2008

Abstract

Prediction of the steady state fly height of air bearing sliders in hard disk drives via simulations plays a big role in the design of such air bearing sliders. Over the past few years slider designs have become increasingly complex with deep etches and steep wall profiles. In this paper we present a novel method of solving the inverse problem for air-bearing sliders in hard disk drives. We also present a new method for calculating the static air-bearing stiffness by solving three linear systems. The formulation is implemented and convergence studies are carried out for the method. Refinements based on flux jumps and pressure gradients are found to work well.

1 Introduction

Hard disk drives today are finding applications well beyond the computer in consumer appliances such as digital video recorders, digital audio players, cameras and PDAs. These appliances are often subject to harsh environments that place stringent requirements on the mechanical performance of such drives. In order to evaluate the designs of air bearings designs and predict their reliability, engineers need fast, reliable simulations not only for their static performance but also for their dynamic flying characteristics during events such as shock, vibration and load/unload. In this paper, we propose and implement an automatic time-stepping unstructured finite element based scheme to solve the time-dependent Reynolds lubrication equation, and use it together with Fe models for the suspension and disk to create a new dynamic simulator.

A good summary of previous work has been presented by Gupta (2007). Many researchers in the past have made attempts to predict the system dynamics using a simple head-disk interface model (Ponnaganti, 1986; Lu, 1997) that includes a simplified slider model and an air-bearing model that solves the generalized Reynolds equation. These models ignore the

dynamic effects of the suspension and the disk. According to Gupta (2007), it has been shown that the system dynamics predicted by these models is significantly different from the actual system response (measured experimentally) during slider-disk contact/impact, aerodynamic forcing on the HSA due to disk rotation, shocks, track-seek and load-unload. Bhargava and Bogy (2007a) used a method in which the structural simulations are carried out in ANSYS, which is a commercial FE Analysis software, and were coupled with air bearing simulations obtained by using the finite volume method for solving the Reynolds equation developed by Hu and Bogy (1995) to simulate the shock response of the suspension/air-bearing/disk system. However this method suffered from computational inefficiency relating to data exchange between ANSYS and air bearing calculations. This method was subsequently improved to include suspension and disk models in the form of reduced mass/stiffness matrices which were used to carry out studies on load/unload (Bhargava and Bogy, 2005), shock (Bhargava and Bogy, 2007b) and aerodynamic forcing Gupta (2007). In this paper, we further improve this simulator by incorporating the FE scheme developed in Part I together with a variable time-stepping scheme based on *a posteriori* error estimates.

2 Methodology

A schematic diagram of the head-disk interface in hard disk drives is shown in Fig. 1. The system consists of an air-bearing slider mounted on a suspension. The slider (which houses the read/write heads) flies in close proximity to the rotating disk, such that the load applied by the suspension is balanced by the air bearing. A typical suspension consists of a stiff load beam and a flexure to which the slider is mounted. The load beam applies a load onto the flexure through a simple pivot contact through the *dimple*. The dimple cannot support negative loads and is often observed to separate from contact during events such as shock and load/unload.

When the slider is flying on the disk, it's motion is governed by the following equations:

$$\mathbf{M}_s\,\ddot{\mathbf{x}}_s + \mathbf{C}_s\,\dot{\mathbf{x}}_s + \mathbf{K}_s\,\mathbf{x}_s + \mathbf{F}_s = \mathbf{F}_{abs}(\mathbf{x}_s - \mathbf{x}_d, \dot{\mathbf{x}}_s - \dot{\mathbf{x}}_d) + \mathbf{F}_{con}(\mathbf{x}_s - \mathbf{x}_d) \tag{1}$$

where $\mathbf{x}$ is the vector of the displacements of the degrees of freedom of the suspension and the 6 degrees of freedom of the slider, namely displacements and rotations in the x, y and z directions (Fig. 2). $\mathbf{M}$, $\mathbf{C}$ and $\mathbf{K}$ correspond to the mass, damping and stiffness matrices for the suspension. $\mathbf{F}_s$ is the preload on the suspension, $\mathbf{F}_{abs}$ is the air-bearing force and $\mathbf{F}_{con}$ is the contact force between the slider and the disk. $\mathbf{F}_{abs}$ and $\mathbf{F}_{con}$ have non-zero values only at the degrees of freedom corresponding to those of the slider. These are calculated by integrating the air-pressure, shear stress, contact pressures and frictional stresses under the slider.

Equation 1 is nonlinear in the displacement vector $\mathbf{x}$. In order to solve this equations, we linearize it and use the Newton Raphson scheme to solve it iteratively to obtain the solution of the corresponding nonlinear problems. Linearizing the dynamic governing equation, Eqn. 1, with respect to $\mathbf{x}$ about a point $\mathbf{x}_0$, we obtain:

$$\begin{aligned}\mathbf{M}\,\partial\ddot{\mathbf{x}} + \mathbf{C}\,\partial\dot{\mathbf{x}} + \mathbf{K}\,\partial\mathbf{x} - \mathbf{C}_{abs}\,\partial\dot{\mathbf{x}} - \mathbf{K}_{abs}\,\partial\mathbf{x} - \mathbf{K}_{con}\,\partial\mathbf{x} = \\ - \mathbf{M}\,\ddot{\mathbf{x}}_0 - \mathbf{C}\,\dot{\mathbf{x}}_0 - \mathbf{K}\,\mathbf{x_0} - \mathbf{F}_{susp} + \mathbf{F}_{abs}(\mathbf{x}_0, \dot{\mathbf{x}}_0) + \mathbf{F}_{con}(\mathbf{x}_0)\end{aligned} \tag{2}$$

where $\partial\mathbf{x} = \mathbf{x} - \mathbf{x}_0$, $\mathbf{C}_{abs}$ and $\mathbf{K}_{abs}$ are the damping and stiffness matrices associated with the air bearing and $\mathbf{K}_{con}$ is the stiffness matrix associated with contact.

The air-bearing pressure used to determine the air-bearing forces and moments is calculated by solving the generalized Reynolds equation. In this section we present the SUPG (Streamline Upwind/Petrov Galerkin) formulation for this equation. The spacing between the slider and the disk is extremely small (much less than the mean free path of air). Under

these conditions, the continuum assumption for the air and the no-slip boundary conditions are no longer valid, and the Reynolds equation is generalized to include rarefaction and slip effects. The generalized time-dependent Reynolds equation can be written in the following form in terms of dimensionless variables, $P = p/p_0$ (pressure normalized with respect to the ambient pressure p_0), $H = h/h_m$ (slider-disk clearance normalized with respect to a nominal spacing h_m) and $T = \omega \cdot t$ (time non-dimensionalized with respect to the angular velocity of the disk, ω):

$$\nabla \cdot (Q\ PH^3\ \nabla P) = \mathbf{\Lambda} \cdot \nabla(PH) + \tau \frac{\partial}{\partial T}(PH) \tag{3}$$

over the domain of the slider ($\mathcal{S}$) along with the boundary condition of ambient pressure ($P = 1$) at the boundary of the slider ($\partial\mathcal{S}$). In the above equation, $\nabla = \frac{\partial}{\partial X}\mathbf{E}_X + \frac{\partial}{\partial Y}\mathbf{E}_Y$ is the gradient operator with respect to normalized coordinates $X = x/L$ and $Y = y/L$ where L is the characteristic length scale for the slider. The non-dimensional vector $\mathbf{\Lambda}$ is the bearing number defined as $\mathbf{\Lambda} = \frac{6\mu \mathbf{U} L}{p_0 h_m^2}$, where μ is the dynamic viscosity of air and $\mathbf{U}$ is the local velocity vector of the disk. The squeeze number τ is defined as $\tau = \frac{12\mu\omega L^2}{p_0 h_m^2}$ and is the ratio of transient effects to the diffusion effects in the problem. The flow factor, Q, is the modification to the continuum generalized Reynolds equation for incorporating slip and rarefaction effects.

To derive the weak form of the dynamic generalized Reynolds equation, Eqn. 3, we multiply the equation by a test function v, integrate over the domain $\mathcal{S}$ and use the divergence theorem to get:

$$\int_{\mathcal{S}} \nabla v \cdot (Q\ PH^3\ \nabla P)\ \mathrm{dA} + \int_{\mathcal{S}} v\ \mathbf{\Lambda} \cdot \nabla(PH)\ \mathrm{dA} + \int_{\mathcal{S}} v\ \tau \frac{\partial}{\partial T}(PH)\ \mathrm{dA} - \int_{\partial\mathcal{S}} v\ (Q\ PH^3\ \nabla P) \cdot \mathbf{n}\ \mathrm{dS} = 0 \tag{4}$$

The above equation along with the boundary condition $P = 1$ over $\partial\mathcal{S}$ is the weak form

of Eqn. 3, and it can be solved to give the pressure field over the slider $\mathcal{S}$. We decompose the domain of the slider $\mathcal{S}$ into a finite number of triangular domains, $\mathcal{T}_i$, the *finite elements*, such that:

$$\mathcal{S} = \bigcup_{i=1}^{N_e} \mathcal{T}_i \quad || \; \mathcal{T}_i \cap \mathcal{T}_j = \emptyset \text{ for } i \neq j \tag{5}$$

Writing the weak form of Eqn. 4 over each element $\mathcal{T}_i$, and applying boundary conditions, we obtain:

$$\int_{\mathcal{T}_i} \nabla v \cdot (Q \; PH^3 \; \nabla P) \; \mathrm{dA} + \int_{\mathcal{T}_i} v \; \mathbf{\Lambda} \cdot \nabla (PH) \; \mathrm{dA} + \int_{\mathcal{T}_i} v \; \tau \left(H \frac{\partial P}{\partial T} + P \frac{\partial H}{\partial T} \right) \; \mathrm{dA} \\ - \int_{\partial \mathcal{T}_i \backslash \partial \mathcal{S}} v \; (Q \; PH^3 \; \nabla P) \cdot \mathbf{n} \; \mathrm{dS} = 0 \tag{6}$$

which is the elemental weak form of the dynamic generalized Reynolds equation.

For the temporal discretization of the dynamic generalized Reynolds equation, we use the trapezoidal rule (see Hairer and Wanner, 1996). This method implies:

$$\dot{P}_{n+1} = 2 \; \frac{P_{n+1} - P_n}{\Delta T_{n+1}} - \dot{P}_n \tag{7}$$

where $\Delta T_{n+1} = T_{n+1} - T_n$. Substituting this into Eqn. 6, we obtain:

$$\int_{\mathcal{T}_i} \nabla v_{n+1} \cdot (Q_{n+1} \; P_{n+1} H_{n+1}^3 \; \nabla P_{n+1}) \; \mathrm{dA} + \int_{\mathcal{T}_i} v_{n+1} \; \mathbf{\Lambda}_{n+1} \cdot \nabla (P_{n+1} H_{n+1}) \; \mathrm{dA} \\ + \int_{\mathcal{T}_i} v_{n+1} \; \tau \left[H_{n+1} \left(2 \; \frac{P_{n+1} - P_n}{\Delta T_{n+1}} - \dot{P}_n \right) + P_{n+1} \dot{H}_{n+1} \right] \; \mathrm{dA} \\ - \int_{\partial \mathcal{T}_i \backslash \partial \mathcal{S}} v_{n+1} \; (Q_{n+1} \; P_{n+1} H_{n+1}^3 \; \nabla P_{n+1}) \cdot \mathbf{n} \; \mathrm{dS} = 0 \tag{8}$$

For simplicity, we drop the subscript from all terms evaluated at T_{n+1} (thus write P_{n+1} as

simply P) and add the subscript '-1' for all terms evaluated at T_n (thus P_n will be written as P_{-1}). The time-step size selection is accomplished by employing an *a posteriori* error estimator proposed by Zienkiewicz and Xie (1991). The time-step size is also reduced during a status change of contact elements and when the slider crashes into the disk.

The weak form of the dynamic generalized Reynolds equation, Eqn. 8, is nonlinear. To solve the nonlinear problem, we utilize the Newton Raphson scheme (see Iserles, 1996), whereby we iteratively solve a series of linearized problems to obtain the solution of the nonlinear problem. In this section we linearize the weak form presented in Eqn. 6 with respect to the pressure P about the pressure P_0[1]. Writing $P = P_0 + \partial P$ and retaining only the linear terms in ∂P we get:

$$\begin{aligned}
&\int_{\mathcal{T}_i} \nabla v \cdot \left(Q\ P_0 H^3\ \nabla P_0 + Q\ P_0 H^3\ \nabla \partial P + Q\ \partial P H^3\ \nabla P_0\right)\ \mathrm{dA} \\
&\qquad + \int_{\mathcal{T}_i} v\ \mathbf{\Lambda} \cdot \left(H\ \nabla P_0 + P_0\ \nabla H + H\ \nabla \partial P + \partial P\ \nabla H\right)\ \mathrm{dA} \\
&\quad + \int_{\mathcal{T}_i} v\ \tau \left(2H\ \frac{P_0 - P_{-1}}{\Delta T} - H \dot{P}_{-1} + 2H \frac{\partial P}{\Delta T} + P_0\ \dot{H} + \partial P\ \dot{H}\right)\ \mathrm{dA} \\
&\qquad - \int_{\partial \mathcal{T}_i \setminus \partial \mathcal{S}} v\ \left(Q\ P_0 H^3\ \nabla P_0 + Q\ P_0 H^3\ \nabla \partial P + Q\ \partial P\ H^3\ \nabla P_0\right) \cdot \mathbf{n}\ \mathrm{dS} = 0 \quad (9)
\end{aligned}$$

We use Eqn. 9 to solve the nonlinear forms using the Newton Raphson scheme.

As seen for the static case in Part I, spurious oscillations are also observed when a regular non-stabilized finite element formulation is used to solve the transient advection-diffusion equation. Hence the SUPG stabilization technique proposed by Brooks and Hughes (1982) discussed in the Part I is also implemented here in the dynamic case.

In order to solve for the pressure field numerically, we approximate it to have a piecewise linear form over each element. We eventually obtain $P = P_i \phi_i^e$ for $i = 1, 2, 3$, where ϕ_i^e are

[1] P_0 is distinct from atmospheric non-dimensional pressure

the local basis functions corresponding to node i. Similarly for the test functions, locally over each element, again we have $v = v_i\widetilde{\phi}_i^e$ for $i = 1, 2, 3$ where $\widetilde{\phi}_i^e$ are the local test basis functions corresponding to node i. Substituting these into Eqn. 9 and collecting the terms, we obtain:

$$\mathbf{v}^{eT}\int\limits_{\mathcal{T}_i}\left[\begin{array}{c} QP_0H^3\,\overline{\mathbf{B}}^e\mathbf{B}^{eT} + QH^3\,\overline{\mathbf{B}}^e\nabla P_0\,\boldsymbol{\phi}^{eT} + H\,\widetilde{\boldsymbol{\phi}}^e\boldsymbol{\Lambda}^T\mathbf{B}^{eT} \\ +\widetilde{\boldsymbol{\phi}}^e\boldsymbol{\Lambda}^T\nabla H\,\boldsymbol{\phi}^{eT} + \tau\left(\dot{H} + \frac{2H}{\Delta T}\right)\widetilde{\boldsymbol{\phi}}^e\boldsymbol{\phi}^{eT} \end{array}\right]\mathrm{dA}\;\partial\mathbf{P}^e$$
$$+\,\mathbf{v}^{eT}\int\limits_{\mathcal{T}_i}\left[\begin{array}{c} QP_0H^3\,\overline{\mathbf{B}}^e\nabla P_0 + H\,\widetilde{\boldsymbol{\phi}}^e\boldsymbol{\Lambda}^T\nabla P_0 + P_0\,\widetilde{\boldsymbol{\phi}}^e\boldsymbol{\Lambda}^T\nabla H \\ +\tau\widetilde{\boldsymbol{\phi}}^e H\dot{P}_{-1} + \tau\widetilde{\boldsymbol{\phi}}^e\frac{2H}{\Delta T}(P_0 - P_{-1}) + \tau\widetilde{\boldsymbol{\phi}}^e P_0\dot{H} \end{array}\right]\mathrm{dA}$$
$$-\,\mathbf{v}^{eT}\int\limits_{\partial\mathcal{T}_i\setminus\partial\mathcal{S}}\widetilde{\boldsymbol{\phi}}^e\,\left(Q\,P_0H^3\,\nabla P_0 + Q\,P_0H^3\,\mathbf{B}^{eT}\partial\mathbf{P}^e + Q\,\boldsymbol{\phi}^{eT}\partial\mathbf{P}^e H^3\,\nabla P_0\right)\cdot\mathbf{n}\,\mathrm{dS} = 0 \quad (10)$$

Since the test functions are arbitrary, Eqn. 10 reduces to the following system of equations:

$$\mathbf{K}^e_{dyn}\,\partial\mathbf{P}^e - \mathbf{R}^e_{dyn} - \int\limits_{\partial\mathcal{T}_i\setminus\partial\mathcal{S}}\widetilde{\boldsymbol{\phi}}^e\,\left(Q\,P_0H^3\,\nabla P_0 + Q\,P_0H^3\,\mathbf{B}^{eT}\partial\mathbf{P}^e + Q\,\boldsymbol{\phi}^{eT}\partial\mathbf{P}^e H^3\,\nabla P_0\right)\cdot\mathbf{n}\,\mathrm{dS} = 0 \quad (11)$$

where $\mathbf{K}^e_{dyn}$ and $\mathbf{R}^e_{dyn}$ are the element stiffness matrix and element flux vector defined as:

$$\mathbf{K}^e_{dyn} = \int\limits_{\mathcal{T}_i}\left[\begin{array}{c} QP_0H^3\,\overline{\mathbf{B}}^e\mathbf{B}^{eT} + QH^3\,\overline{\mathbf{B}}^e\nabla P_0\,\boldsymbol{\phi}^{eT} + H\,\widetilde{\boldsymbol{\phi}}^e\boldsymbol{\Lambda}^T\mathbf{B}^{eT} \\ +\widetilde{\boldsymbol{\phi}}^e\boldsymbol{\Lambda}^T\nabla H\,\boldsymbol{\phi}^{eT} + \tau\left(\dot{H} + \frac{2H}{\Delta T}\right)\widetilde{\boldsymbol{\phi}}^e\boldsymbol{\phi}^{eT} \end{array}\right]\mathrm{dA} \quad (12)$$

$$\mathbf{R}^e_{dyn} = -\int\limits_{\mathcal{T}_i}\left[\begin{array}{c} QP_0H^3\,\overline{\mathbf{B}}^e\nabla P_0 + H\,\widetilde{\boldsymbol{\phi}}^e\boldsymbol{\Lambda}^T\nabla P_0 + P_0\,\widetilde{\boldsymbol{\phi}}^e\boldsymbol{\Lambda}^T\nabla H \\ +\tau\widetilde{\boldsymbol{\phi}}^e H\dot{P}_{-1} + \tau\widetilde{\boldsymbol{\phi}}^e\frac{2H}{\Delta T}(P_0 - P_{-1}) + \tau\widetilde{\boldsymbol{\phi}}^e P_0\dot{H} \end{array}\right]\mathrm{dA} \quad (13)$$

The Reynolds equation is solved in a Lagrangian frame and the spatial mesh is fixed during the temporal solution. The spatial mesh used is obtained from the solution of the steady state problem presented in Part I.

In order to obtain the complete pressure profile over the slider $\mathcal{S}$, we need to solve Eqn. 11 simultaneously over all of the elements. Thus the equations are assembled to form the global stiffness matrix and the global flux vector. During assembly, the flux discontinuities between the elements, accounted for by the third term in Eqn. 11, are neglected, and hence the global system of equations obtained can be written as:

$$\mathbf{K}\,\partial\mathbf{P} = \mathbf{R} \tag{14}$$

where, $\mathbf{K} = \mathbf{K}_{dyn} = \mathop{\mathrm{A}}_{i=1}^{N_e} \mathbf{K}^e_{dyn}$, $\mathbf{R} = \mathbf{R}_{dyn} = \mathop{\mathrm{A}}_{i=1}^{N_e} \mathbf{R}^e_{dyn}$ for the dynamic case, $\partial\mathbf{P} = \mathop{\mathrm{A}}_{i=1}^{N_e} \partial\mathbf{P}^e$ and A is the assembly operator.

The resulting sparse linear system of equations is renumbered to form a banded matrix and the resulting system is solved using a preconditioned GMRES technique similar to the one used for the static case in Part I.

Next we are concerned with the calculation of the air-bearing damping and stiffness matrices. These are defined as the changes in forces and moments of the air-bearing due to changes in the flying attitude and velocities of the slider. To determine these, we need to find the change in pressure P due to changes in the attitude/velocity of the slider. The clearance H under the slider depends on the attitude of the slider as:

$$H = \frac{1}{h_m}\left(d_{etch} + z_{pivot} + XL \cdot \theta_{pitch} + YL \cdot \theta_{roll}\right) \tag{15}$$

where d_{etch} is the etch depth, z_{pivot} is the z-height of the pivot location, θ_{pitch} is the pitch angle and θ_{roll} is the roll angle, and X and Y are the coordinates of the point measured from the pivot location (see Fig. 2). Similarly the time derivatives of the clearance $\dot{H}$ depend on

the velocity of the slider as:

$$\dot{H} = \frac{1}{h_m}\left(\dot{z}_{pivot} + XL \cdot \dot{\theta}_{pitch} + YL \cdot \dot{\theta}_{roll}\right) \tag{16}$$

Now we can write the weak form of the generalized Reynolds equation, Eqn. 4 as some function ϑ of pressures, clearance and their derivatives as:

$$\vartheta(P, H, \dot{P}, \dot{H}) = 0 \tag{17}$$

To calculate the stiffness, we differentiate this expression with respect to the slider attitude. Differentiating with respect to z_{pivot}, we get:

$$\frac{\mathrm{d}\vartheta(P, H, \dot{P}, \dot{H})}{\mathrm{d}z_{pivot}} = \frac{\partial\vartheta(P, H, \dot{P}, \dot{H})}{\partial H} \cdot \frac{\partial H}{\partial z_{pitch}} + \frac{\partial\vartheta(P, H, \dot{P}, \dot{H})}{\partial P} \cdot \frac{\mathrm{d}P}{\mathrm{d}z_{pivot}} = 0 \tag{18}$$

$$\Rightarrow \frac{\mathrm{d}P}{\mathrm{d}z_{pivot}} = \left[\frac{\partial\vartheta(P, H, \dot{P}, \dot{H})}{\partial P}\right]^{-1} \left\{\frac{\partial\vartheta(P, H, \dot{P}, \dot{H})}{\partial H} \cdot \frac{\partial H}{\partial z_{pivot}}\right\} \tag{19}$$

In the above formulation, we are neglect the dependence of $\dot{P}$ on the slider's attitude H. Similarly differentiating with respect to θ_{pitch} and θ_{roll}, we obtain:

$$\frac{\mathrm{d}P}{\mathrm{d}\theta_{pitch}} = \left[\frac{\partial\vartheta(P, H, \dot{P}, \dot{H})}{\partial P}\right]^{-1} \left\{\frac{\partial\vartheta(P, H, \dot{P}, \dot{H})}{\partial H} \cdot \frac{\partial H}{\partial \theta_{pitch}}\right\} \tag{20}$$

$$\frac{\mathrm{d}P}{\mathrm{d}\theta_{roll}} = \left[\frac{\partial\vartheta(P, H, \dot{P}, \dot{H})}{\partial P}\right]^{-1} \left\{\frac{\partial\vartheta(P, H, \dot{P}, \dot{H})}{\partial H} \cdot \frac{\partial H}{\partial \theta_{roll}}\right\} \tag{21}$$

Substituting the finite element interpolations into these expressions and evaluating the

results, we get:

$$\left\{\frac{\mathrm{d}\mathbf{P}}{\mathrm{d}z_{pivot}}\right\} = \left[\,\mathbf{K}_{stat}\,\right]^{-1}\left\{\frac{\partial\mathbf{R_{stat}}}{\partial z_{pivot}}\right\} \tag{22}$$

$$\left\{\frac{\mathrm{d}\mathbf{P}}{\mathrm{d}\theta_{pitch}}\right\} = \left[\,\mathbf{K}_{stat}\,\right]^{-1}\left\{\frac{\partial\mathbf{R_{stat}}}{\partial \theta_{pitch}}\right\} \tag{23}$$

$$\left\{\frac{\mathrm{d}\mathbf{P}}{\mathrm{d}\theta_{roll}}\right\} = \left[\,\mathbf{K}_{stat}\,\right]^{-1}\left\{\frac{\partial\mathbf{R_{stat}}}{\partial \theta_{roll}}\right\} \tag{24}$$

where $\mathbf{K}_{stat}$ is the global steady state stiffness matrix and the vectors $\frac{\partial\mathbf{R}_{stat}}{\partial z_{pivot}}$, $\frac{\partial\mathbf{R}_{stat}}{\partial \theta_{pitch}}$ and $\frac{\partial\mathbf{R}_{stat}}{\partial \theta roll}$ are defined as:

$$\left\{\frac{\partial\mathbf{R_{stat}}}{\partial z_{pivot}}\right\} = -\frac{1}{h_m}\sum_{i=1}^{N_e}\int_{\mathcal{T}_i}(3\;QP_0H^2\;\overline{\mathbf{B}}^e\nabla P_0 + \widetilde{\boldsymbol{\phi}}^e\boldsymbol{\Lambda}^T\nabla P_0)\;\mathrm{dA} \tag{25}$$

$$\left\{\frac{\partial\mathbf{R_{stat}}}{\partial \theta_{pitch}}\right\} = -\frac{L}{h_m}\sum_{i=1}^{N_e}\int_{\mathcal{T}_i}(3\;QP_0H^2\;\overline{\mathbf{B}}^e\nabla P_0 + \widetilde{\boldsymbol{\phi}}^e\boldsymbol{\Lambda}^T\nabla P_0)\cdot X\;\mathrm{dA} \tag{26}$$

$$\left\{\frac{\partial\mathbf{R_{stat}}}{\partial \theta_{roll}}\right\} = -\frac{L}{h_m}\sum_{i=1}^{N_e}\int_{\mathcal{T}_i}(3\;QP_0H^2\;\overline{\mathbf{B}}^e\nabla P_0 + \widetilde{\boldsymbol{\phi}}^e\boldsymbol{\Lambda}^T\nabla P_0)\cdot Y\;\mathrm{dA} \tag{27}$$

The above expressions hold for both the time dependent and the steady state versions of the Reynolds equation. The terms of the 3×3 stiffness matrix can then be evaluated as:

$$\mathbf{K}_{abs} = \begin{bmatrix} \mathbf{C}_{F_z}^T\left\{\frac{\partial\mathbf{R}_{stat}}{\partial z_{pivot}}\right\} & \mathbf{C}_{M_{pitch}}^T\left\{\frac{\partial\mathbf{R}_{stat}}{\partial z_{pivot}}\right\} & \mathbf{C}_{M_{roll}}^T\left\{\frac{\partial\mathbf{R}_{stat}}{\partial z_{pivot}}\right\} \\ \mathbf{C}_{F_z}^T\left\{\frac{\partial\mathbf{R}_{stat}}{\partial \theta_{pitch}}\right\} & \mathbf{C}_{M_{pitch}}^T\left\{\frac{\partial\mathbf{R}_{stat}}{\partial \theta_{pitch}}\right\} & \mathbf{C}_{M_{pitch}}^T\left\{\frac{\partial\mathbf{R}_{stat}}{\partial \theta_{pitch}}\right\} \\ \mathbf{C}_{F_z}^T\left\{\frac{\partial\mathbf{R}_{stat}}{\partial \theta_{roll}}\right\} & \mathbf{C}_{M_{pitch}}^T\left\{\frac{\partial\mathbf{R}_{stat}}{\partial \theta_{roll}}\right\} & \mathbf{C}_{M_{roll}}^T\left\{\frac{\partial\mathbf{R}_{stat}}{\partial \theta_{roll}}\right\} \end{bmatrix} \tag{28}$$

Thus the stiffness is obtained by the solution of three extra linear systems. However this is not computationally very expensive even with iterative methods (where the system matrix $\mathbf{K}$ has not been factorized) since preconditioners for $\mathbf{K}$ will already have been evaluated.

Now we consider the damping matrix evaluation. Again we consider Eqn. 17. This time,

we differentiate with respect to the time derivative of the clearance $\dot{H}$ and velocities of the slider attitudes. Differentiating with respect to $\dot{z}_{pivot}$, we obtain:

$$\frac{\mathrm{d}\vartheta(P,H,\dot{P},\dot{H})}{\mathrm{d}\dot{z}_{pivot}} = \frac{\partial\vartheta(P,H,\dot{P},\dot{H})}{\partial\dot{H}} \cdot \frac{\partial\dot{H}}{\partial\dot{z}_{pitch}} + \frac{\partial\vartheta(P,H,\dot{P},\dot{H})}{\partial P} \cdot \frac{\mathrm{d}P}{\mathrm{d}\dot{z}_{pivot}} = 0 \tag{29}$$

$$\Rightarrow \frac{\mathrm{d}P}{\mathrm{d}\dot{z}_{pivot}} = \left[\frac{\partial\vartheta(P,H,\dot{P},\dot{H})}{\partial P}\right]^{-1} \left\{\frac{\partial\vartheta(P,H,\dot{P},\dot{H})}{\partial\dot{H}} \cdot \frac{\partial\dot{H}}{\partial\dot{z}_{pivot}}\right\} \tag{30}$$

Again, we neglect the dependence of $\dot{P}$ on $\dot{H}$. This assumption is reasonable when the slider is close to the steady state fly height. Similarly differentiating with respect to $\dot{\theta}_{pitch}$ and $\dot{\theta}_{roll}$, we obtain:

$$\frac{\mathrm{d}P}{\mathrm{d}\dot{\theta}_{pitch}} = \left[\frac{\partial\vartheta(P,H,\dot{P},\dot{H})}{\partial P}\right]^{-1} \left\{\frac{\partial\vartheta(P,H,\dot{P},\dot{H})}{\partial\dot{H}} \cdot \frac{\partial\dot{H}}{\partial\dot{\theta}_{pitch}}\right\} \tag{31}$$

$$\frac{\mathrm{d}P}{\mathrm{d}\dot{\theta}_{roll}} = \left[\frac{\partial\vartheta(P,H,\dot{P},\dot{H})}{\partial P}\right]^{-1} \left\{\frac{\partial\vartheta(P,H,\dot{P},\dot{H})}{\partial\dot{H}} \cdot \frac{\partial\dot{H}}{\partial\dot{\theta}_{roll}}\right\} \tag{32}$$

Substituting the finite element interpolations and evaluating the expressions above, we get:

$$\left\{\frac{\mathrm{d}\mathbf{P}}{\mathrm{d}\dot{z}_{pivot}}\right\} = [\mathbf{K}_{stat}]^{-1} \left\{\frac{\partial\mathbf{R}_{\mathbf{dyn}}}{\partial\dot{z}_{pivot}}\right\} \tag{33}$$

$$\left\{\frac{\mathrm{d}\mathbf{P}}{\mathrm{d}\dot{\theta}_{pitch}}\right\} = [\mathbf{K}_{stat}]^{-1} \left\{\frac{\partial\mathbf{R}_{\mathbf{dyn}}}{\partial\dot{\theta}_{pitch}}\right\} \tag{34}$$

$$\left\{\frac{\mathrm{d}\mathbf{P}}{\mathrm{d}\dot{\theta}_{roll}}\right\} = [\mathbf{K}_{stat}]^{-1} \left\{\frac{\partial\mathbf{R}_{\mathbf{dyn}}}{\partial\dot{\theta}_{roll}}\right\} \tag{35}$$

where $\mathbf{K}_{stat}$ is the global steady state stiffness matrix and the vectors $\frac{\partial\mathbf{R}_{dyn}}{\partial\dot{z}_{pivot}}$, $\frac{\partial\mathbf{R}_{dyn}}{\partial\dot{\theta}_{pitch}}$ and $\frac{\partial\mathbf{R}_{dyn}}{\partial\dot{\theta}roll}$

are defined as:

$$\left\{\frac{\partial \mathbf{R_{dyn}}}{\partial \dot{z}_{pivot}}\right\} = -\frac{1}{h_m} \mathop{\mathrm{A}}_{i=1}^{N_e} \int_{\mathcal{T}_i} (\tau P \widetilde{\boldsymbol{\phi}}^e) \, \mathrm{dA} \tag{36}$$

$$\left\{\frac{\partial \mathbf{R_{dyn}}}{\partial \dot{\theta}_{pitch}}\right\} = -\frac{L}{h_m} \mathop{\mathrm{A}}_{i=1}^{N_e} \int_{\mathcal{T}_i} (\tau P \widetilde{\boldsymbol{\phi}}^e) \cdot X \, \mathrm{dA} \tag{37}$$

$$\left\{\frac{\partial \mathbf{R_{dyn}}}{\partial \dot{\theta}_{roll}}\right\} = -\frac{L}{h_m} \mathop{\mathrm{A}}_{i=1}^{N_e} \int_{\mathcal{T}_i} (\tau P \widetilde{\boldsymbol{\phi}}^e) \cdot Y \, \mathrm{dA} \tag{38}$$

The terms of the 3×3 damping matrix can then be evaluated as:

$$\mathbf{C}_{abs} = \begin{bmatrix} \mathbf{C}_{F_z}^T \left\{\frac{\partial \mathbf{R}_{dyn}}{\partial \dot{z}_{pivot}}\right\} & \mathbf{C}_{M_{pitch}}^T \left\{\frac{\partial \mathbf{R}_{dyn}}{\partial \dot{z}_{pivot}}\right\} & \mathbf{C}_{M_{roll}}^T \left\{\frac{\partial \mathbf{R}_{dyn}}{\partial \dot{z}_{pivot}}\right\} \\ \mathbf{C}_{F_z}^T \left\{\frac{\partial \mathbf{R}_{dyn}}{\partial \dot{\theta}_{pitch}}\right\} & \mathbf{C}_{M_{pitch}}^T \left\{\frac{\partial \mathbf{R}_{dyn}}{\partial \dot{\theta}_{pitch}}\right\} & \mathbf{C}_{M_{pitch}}^T \left\{\frac{\partial \mathbf{R}_{dyn}}{\partial \dot{\theta}_{pitch}}\right\} \\ \mathbf{C}_{F_z}^T \left\{\frac{\partial \mathbf{R}_{dyn}}{\partial \dot{\theta}_{roll}}\right\} & \mathbf{C}_{M_{pitch}}^T \left\{\frac{\partial \mathbf{R}_{dyn}}{\partial \dot{\theta}_{roll}}\right\} & \mathbf{C}_{M_{roll}}^T \left\{\frac{\partial \mathbf{R}_{dyn}}{\partial \dot{\theta}_{roll}}\right\} \end{bmatrix} \tag{39}$$

We now consider the evaluation of the algorithmic air-bearing stiffness, which will be used to solve the nonlinear time-discretized Reynolds equation. The algorithmic stiffness matrix is defined as the change in forces and moments of the air-bearing due to changes in the flying attitude of the slider after time discretization has been done. Proceeding in a fashion similar to the previous section, we get:

$$\left\{\frac{\mathrm{d}\mathbf{P}}{\mathrm{d}z_{pivot}}\right\} = [\mathbf{K}_{dyn}]^{-1} \left\{\frac{\partial \mathbf{R}_{dyn}}{\partial z_{pivot}}\right\} \tag{40}$$

$$\left\{\frac{\mathrm{d}\mathbf{P}}{\mathrm{d}\theta_{pitch}}\right\} = [\mathbf{K}_{dyn}]^{-1} \left\{\frac{\partial \mathbf{R}_{dyn}}{\partial \theta_{pitch}}\right\} \tag{41}$$

$$\left\{\frac{\mathrm{d}\mathbf{P}}{\mathrm{d}\theta_{roll}}\right\} = [\mathbf{K}_{dyn}]^{-1} \left\{\frac{\partial \mathbf{R}_{dyn}}{\partial \theta_{roll}}\right\} \tag{42}$$

where $\mathbf{K}_{dyn}$ is the global dynamic stiffness matrix and the vectors $\frac{\partial \mathbf{R}_{dyn}}{\partial z_{pivot}}$, $\frac{\partial \mathbf{R}_{dyn}}{\partial \theta_{pitch}}$ and $\frac{\partial \mathbf{R}_{dyn}}{\partial \theta roll}$

are defined as:

$$\left\{\frac{\partial \mathbf{R}_{dyn}}{\partial z_{pivot}}\right\} = -\sum_{i=1}^{N_e} \int_{\mathcal{T}_i} \left[\begin{array}{c} 3\,Q P_0 H^2\,\overline{\mathbf{B}}^e \nabla P_0 + \widetilde{\boldsymbol{\phi}}^e \boldsymbol{\Lambda}^T \nabla P_0 + P_0\,\widetilde{\boldsymbol{\phi}}^e \boldsymbol{\Lambda}^T \mathbf{B}^{eT} \\ +\tau \widetilde{\boldsymbol{\phi}}^e \dot{P}_{-1} + \tau \widetilde{\boldsymbol{\phi}}^e \frac{2}{\Delta T}(2P_0 - P_{-1}) \end{array}\right] \mathrm{dA} \tag{43}$$

$$\left\{\frac{\partial \mathbf{R}_{dyn}}{\partial \theta_{pitch}}\right\} = -\sum_{i=1}^{N_e} \int_{\mathcal{T}_i} \left[\begin{array}{c} 3\,Q P_0 H^2\,\overline{\mathbf{B}}^e \nabla P_0 + \widetilde{\boldsymbol{\phi}}^e \boldsymbol{\Lambda}^T \nabla P_0 + P_0\,\widetilde{\boldsymbol{\phi}}^e \boldsymbol{\Lambda}^T \mathbf{B}^{eT} \\ +\tau \widetilde{\boldsymbol{\phi}}^e \dot{P}_{-1} + \tau \widetilde{\boldsymbol{\phi}}^e \frac{2}{\Delta T}(2P_0 - P_{-1}) \end{array}\right] \cdot X \ \mathrm{dA} \tag{44}$$

$$\left\{\frac{\partial \mathbf{R}_{dyn}}{\partial \theta_{roll}}\right\} = -\sum_{i=1}^{N_e} \int_{\mathcal{T}_i} \left[\begin{array}{c} 3\,Q P_0 H^2\,\overline{\mathbf{B}}^e \nabla P_0 + \widetilde{\boldsymbol{\phi}}^e \boldsymbol{\Lambda}^T \nabla P_0 + P_0\,\widetilde{\boldsymbol{\phi}}^e \boldsymbol{\Lambda}^T \mathbf{B}^{eT} \\ +\tau \widetilde{\boldsymbol{\phi}}^e \dot{P}_{-1} + \tau \widetilde{\boldsymbol{\phi}}^e \frac{2}{\Delta T}(2P_0 - P_{-1}) \end{array}\right] \cdot Y \ \mathrm{dA} \tag{45}$$

Again, the terms of the 3×3 stiffness matrix can then be evaluated as:

$$\mathbf{K}_{alg} = \left[\begin{array}{ccc} \mathbf{C}_{F_z}^T \left\{\frac{\partial \mathbf{R}_{dyn}}{\partial z_{pivot}}\right\} & \mathbf{C}_{M_{pitch}}^T \left\{\frac{\partial \mathbf{R}_{dyn}}{\partial z_{pivot}}\right\} & \mathbf{C}_{M_{roll}}^T \left\{\frac{\partial \mathbf{R}_{dyn}}{\partial z_{pivot}}\right\} \\ \mathbf{C}_{F_z}^T \left\{\frac{\partial \mathbf{R}_{dyn}}{\partial \theta_{pitch}}\right\} & \mathbf{C}_{M_{pitch}}^T \left\{\frac{\partial \mathbf{R}_{dyn}}{\partial \theta_{pitch}}\right\} & \mathbf{C}_{M_{pitch}}^T \left\{\frac{\partial \mathbf{R}_{dyn}}{\partial \theta_{pitch}}\right\} \\ \mathbf{C}_{F_z}^T \left\{\frac{\partial \mathbf{R}_{dyn}}{\partial \theta_{roll}}\right\} & \mathbf{C}_{M_{pitch}}^T \left\{\frac{\partial \mathbf{R}_{dyn}}{\partial \theta_{roll}}\right\} & \mathbf{C}_{M_{roll}}^T \left\{\frac{\partial \mathbf{R}_{dyn}}{\partial \theta_{roll}}\right\} \end{array}\right] \tag{46}$$

The algorithmic stiffness matrix is used in place of the stiffness and damping matrices for Newton's iterations for the equations of motion, since it is a more accurate representation of the stiffness of the time-discretized generalized Reynolds equation.

3 Numerical Simulations

Here the methodology discussed in the previous sections is implemented. We present simulations of free vibrations, shock and the unloading process of the suspension/air-bearing/disk system. The slider design used in this simulation is shown in Fig. 3. The slider is loaded onto a disk spinning at 3600 RPM at a radius of 13 mm. The slider has a pitch static attitude of 2.5 mrad and zero roll static attitude.

The first simulation is for free vibrations. The initial conditions provided to the system

are perturbed from the steady state, and the resulting free vibrations of the system are simulated. The slider's fly-height, pitch and roll are plotted in Fig. 4 along with the z-force and pitch/roll moments in Fig. 5. In Fig. 6, we plot the error estimate and the time-step size. We observe that during the initial large amplitude oscillations, the time step is small, and, it gradually increases as the oscillations are damped out.

Next, we present results from a shock simulation. Shocks are simulated as acceleration pulses to the structural components of the system, i.e. the suspension and the disk. In this case we apply a half-sine pulse of 300 G amplitude and a pulse width of 0.2 ms. The slider attitude is plotted in Fig. 7. In this case we observe that the head-disk interface is fairly resilient to the shock pulse and there is no head-disk contact. In Fig. 8 we show the forces and moments on the slider and in Fig. 9, we plot the contact forces at the dimple. We see that the dimple contact force is always positive and the dimple does not open.

The final simulation presented here is for the unloading process. The unloading process is simulated by moving the actuator over a ramp. The slider's attitude in this case is plotted in Fig. 11. We observe that the unloading takes place at about 2.7 ms. In Fig. 12 we plot the suspension, air-bearing and contact forces during the unloading process. We observe that the unloading process begins at about 0.6 ms when the L/UL tab contacts the ramp (see Fig. 14). At about 0.8 ms, the dimple opens, which can be seen from the dimple contact force in Fig. 13, as well as from the change in the 'degramming' rate seen in Fig. 12 a). The error estimate and the time step are plotted in Fig. 15.

4 Summary and Conclusion

In this Part II paper we presented a new finite element formulation developed for simulating the head-disk interface in hard disk drives under dynamic disturbances. The coupled structural-fluid problem is solved via a linearized iteration scheme. We use a variable time-

step discretization scheme to advance the equation in time. Expressions are derived for the stiffness, damping and the algorithmic stiffness. The method is implemented and simulation results are presented for various dynamic events including the unloading process and shock.

Acknowledgment

This study was supported by Seagate Corporation and the Computer Mechanics Laboratory (CML) at the University of California, Berkeley.

References

P. Bhargava and D. B. Bogy. Numerical simulation of load/unload in small form factor hard disk drives. Technical Report 2005-011, CML, University of California, Berkeley, 2005.

P. Bhargava and D. B. Bogy. Numerical simulation of operational-shock in small form factor hard disk drives. *Journal of Tribology*, 129(1):153–160, 2007a.

P. Bhargava and D. B. Bogy. Effect of shock pulse width on the shock response of small form factor disk drives. *Microsystem Technologies*, 13(8-10):1107–1115, 2007b.

A. N. Brooks and T. J. R. Hughes. Streamline Upwind/Petrov-Galerkin formulations for convection dominated flows with particular emphasis on the incompressible navier-stokes equations. *Computer methods in applied mechanics and engineering*, 32:199–259, 1982.

V. Gupta. *Air Bearing slider dynamics and stability in hard disk drives*. PhD thesis, University of California, Berkeley, 2007.

E. Hairer and G. Wanner. *Solving Ordinary Differential Equations II*. Springer, 1996.

Y. Hu and D. B. Bogy. The cml air bearing dynamic simulator. Technical Report 1995-011, CML, University of California, Berkeley, 1995.

A. Iserles. *A First Course in the Numerical Analysis of Differential Equations*. Cambridge University Press, 1996.

S. Lu. *Numerical Simulation of Slider Air Bearings*. PhD thesis, University of California, Berkeley, 1997.

V. Ponnaganti. *Dynamics of Head-Disk Interaction in Magnetic Recording*. PhD thesis, Stanford University, 1986.

O. C. Zienkiewicz and Y. M. Xie. A simple error estimator and adaptive time stepping procedure for dynamic analysis. *Earthquake Engineering and Structural Dynamics*, 20: 871–887, 1991.

5 Figures

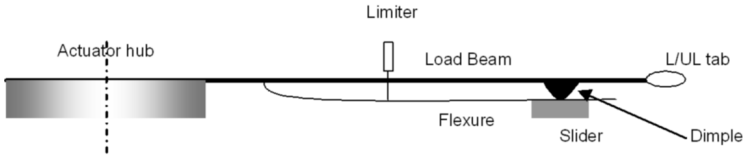

Figure 1: Schematic of the head-disk interface

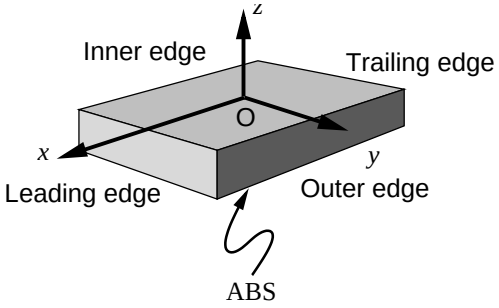

Figure 2: System Coordinate System

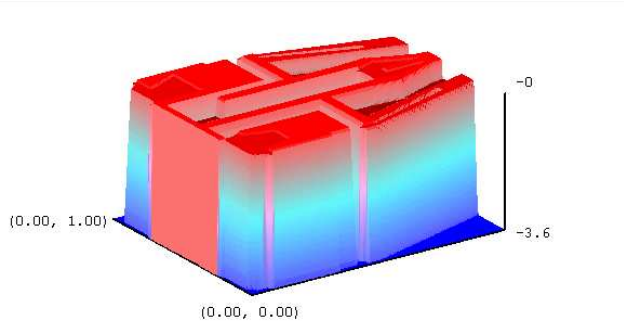

Figure 3: Slider 2

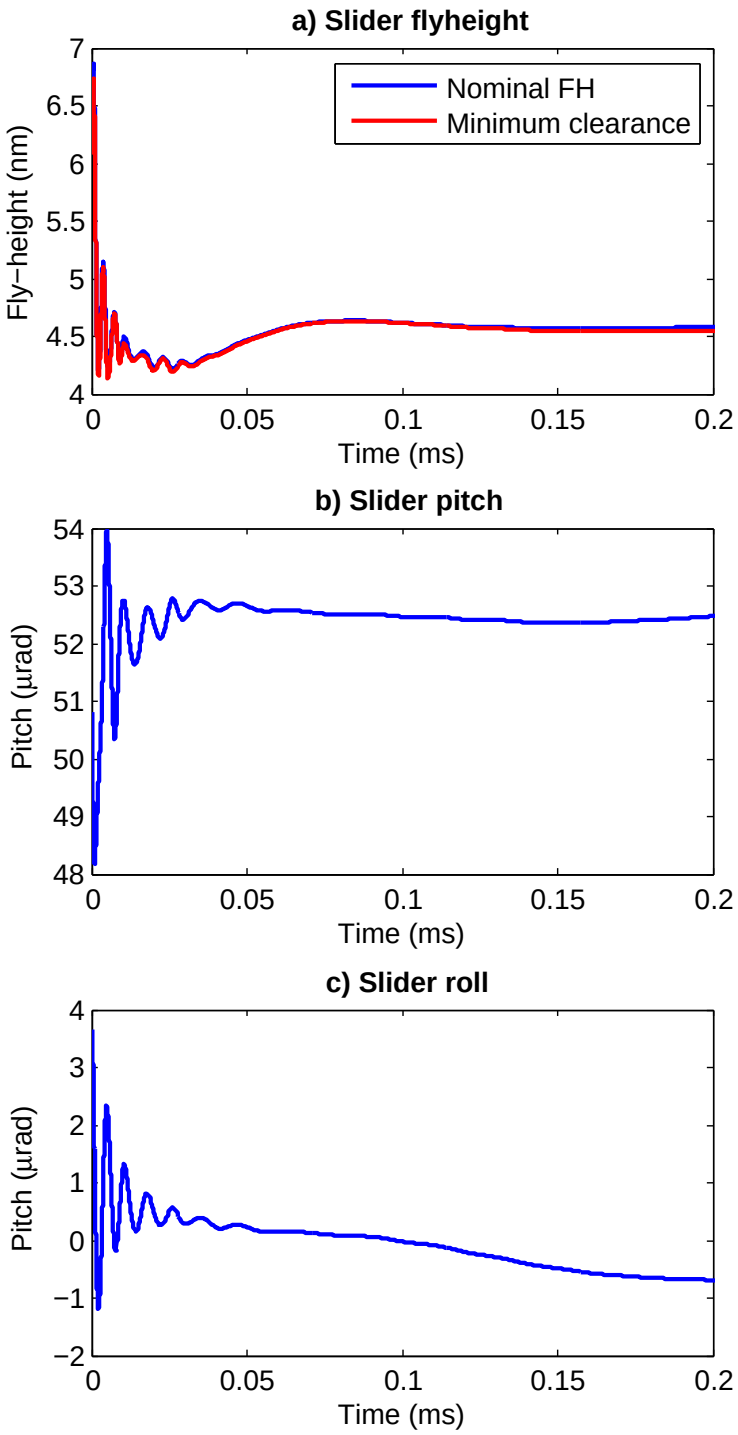

Figure 4: Slider attitude for free vibration simulation

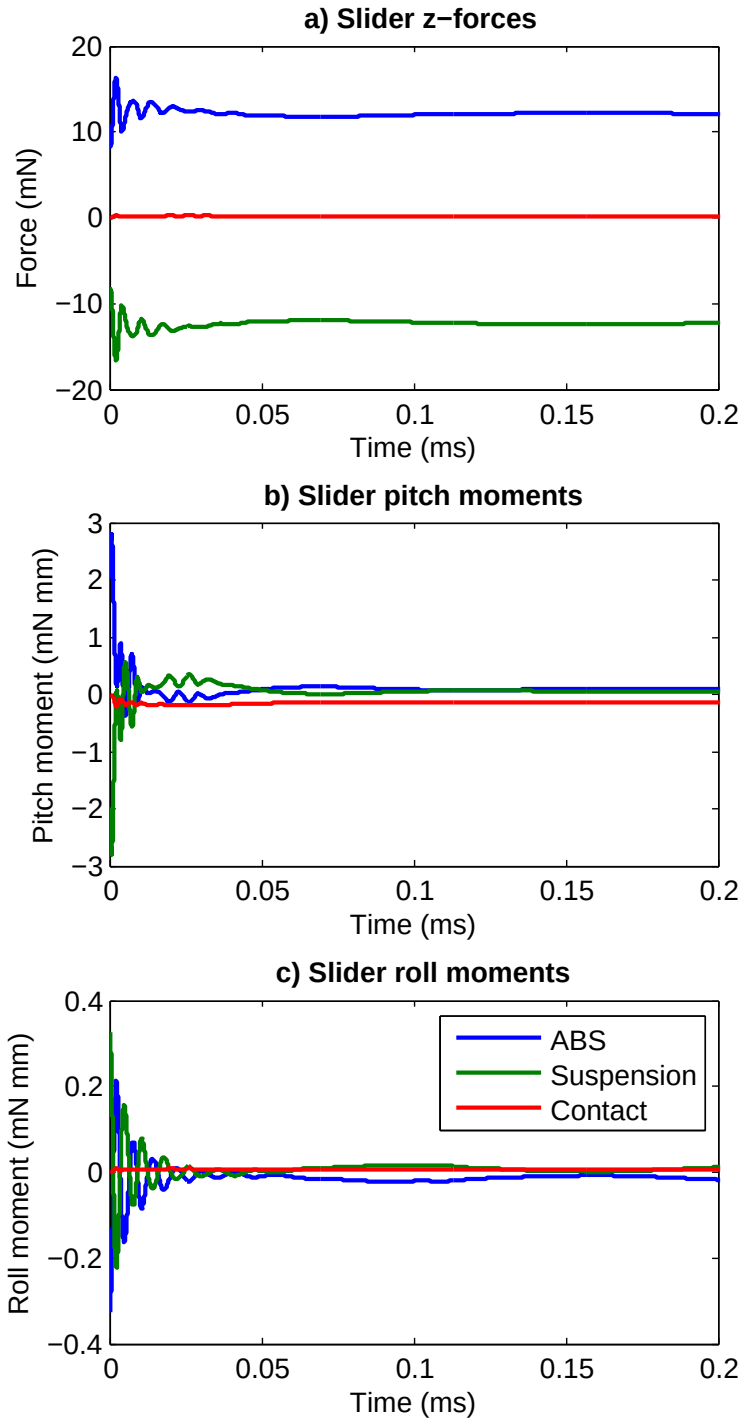

Figure 5: Slider forces for free vibration simulation

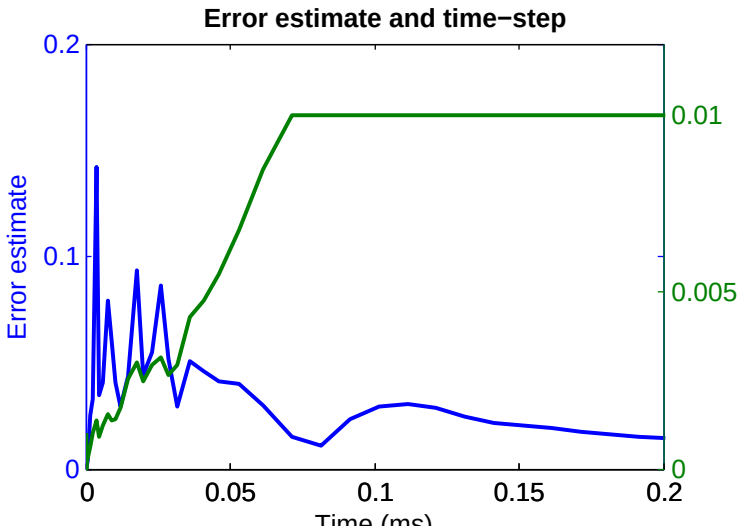

Figure 6: Error-estimate/time-step for free vibration simulation

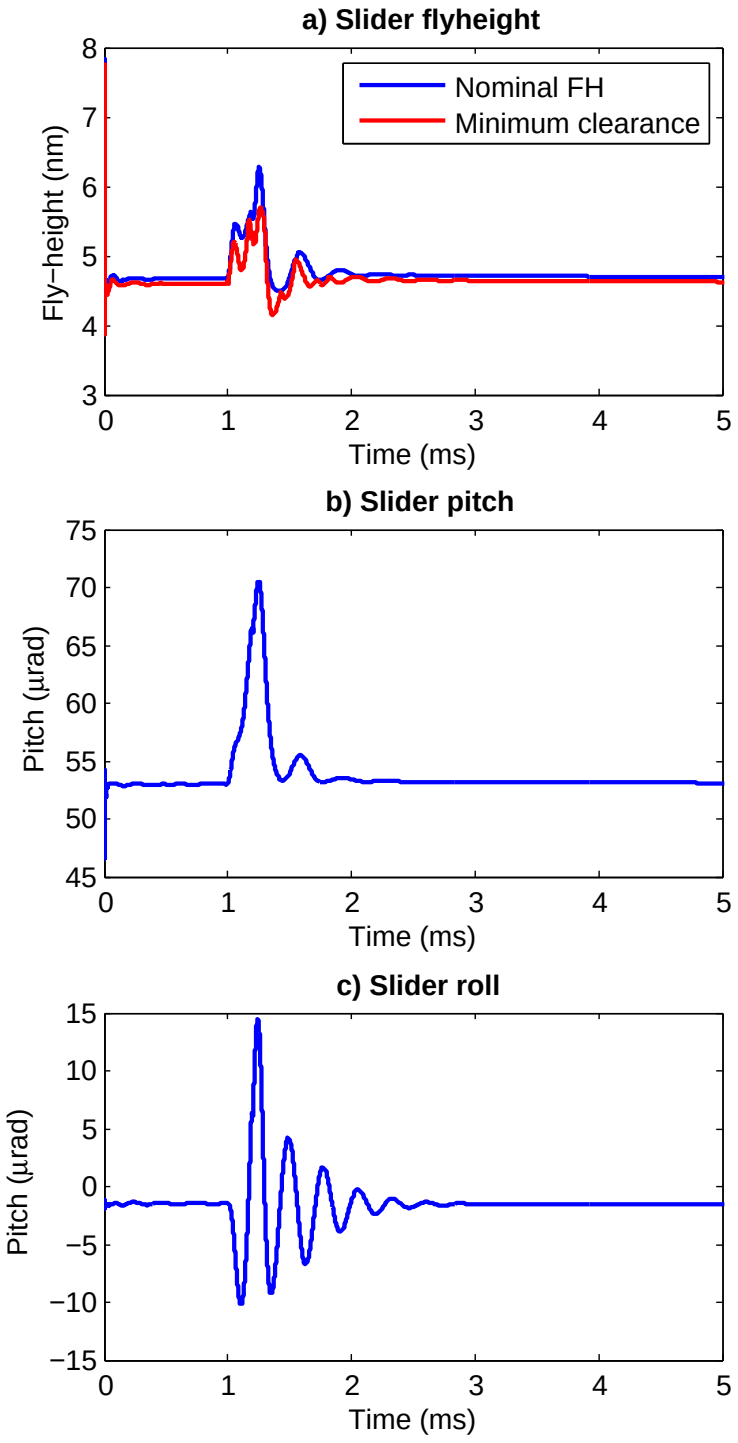

Figure 7: Slider attitude for shock simulation

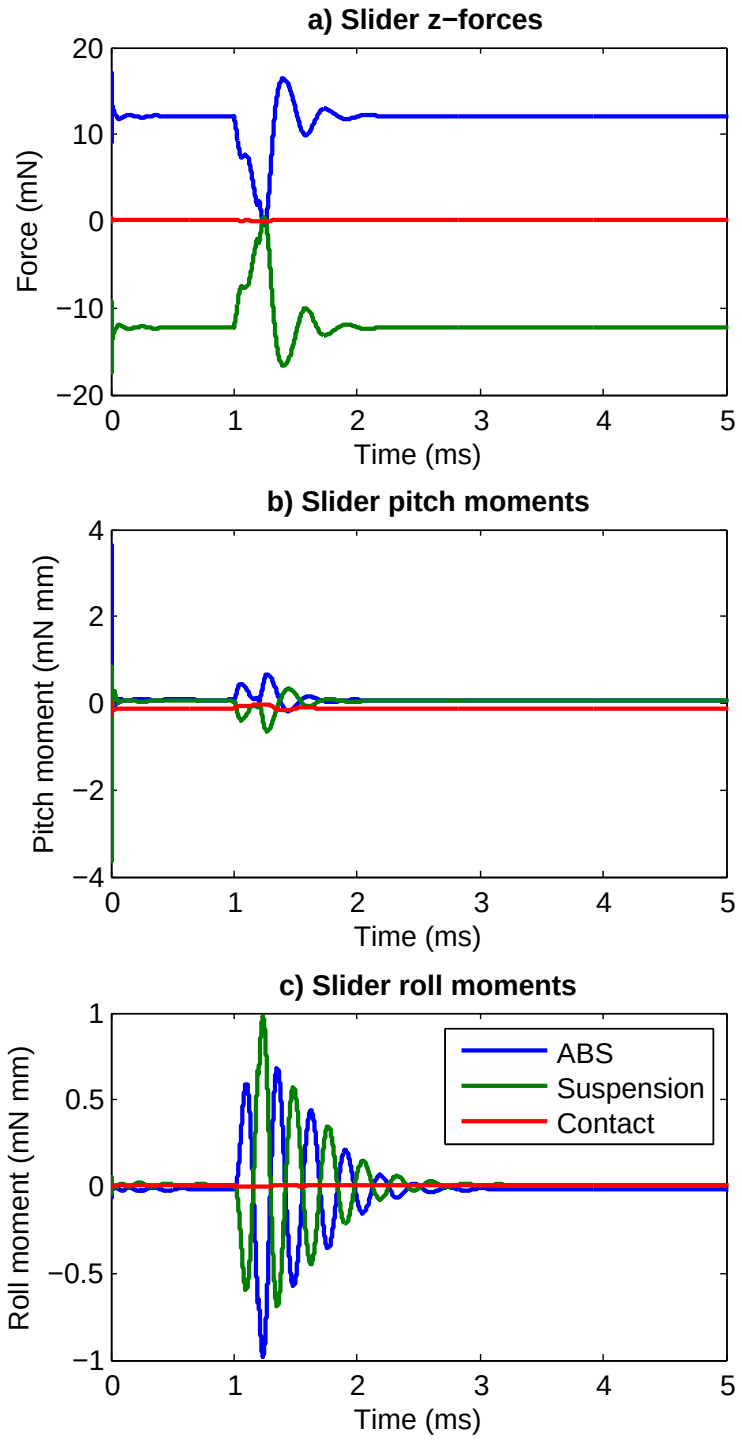

Figure 8: Slider forces for shock simulation

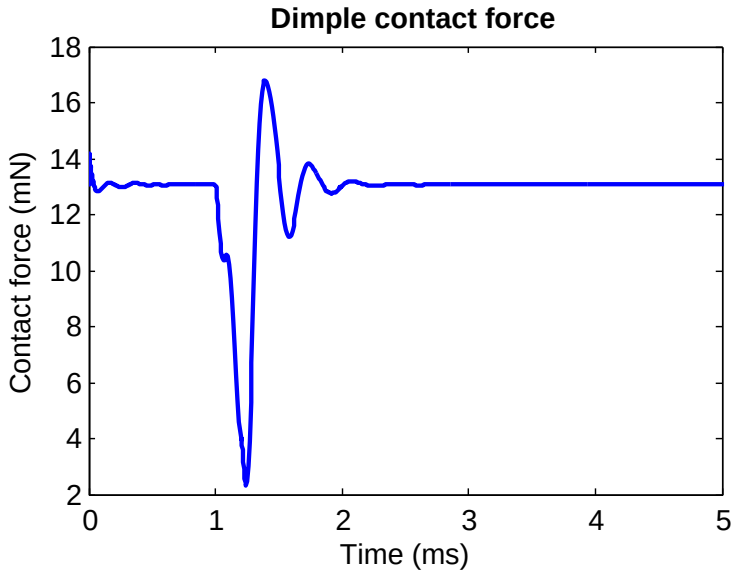

Figure 9: Dimple contact force for shock simulation

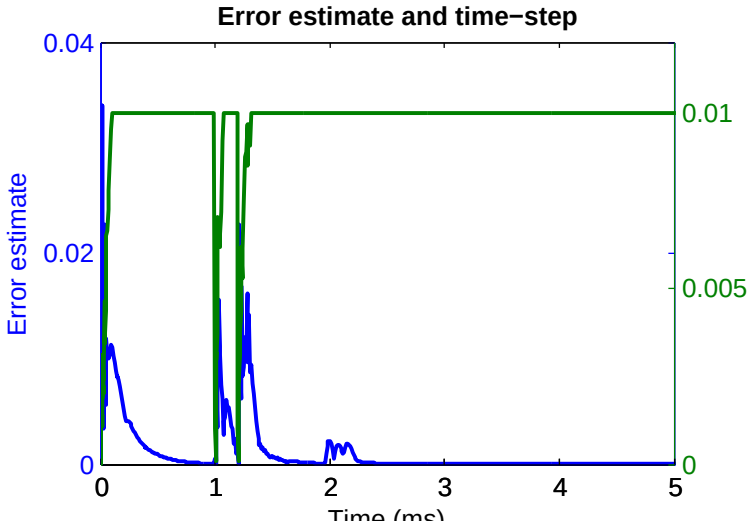

Figure 10: Error-estimate/time-step for shock simulation

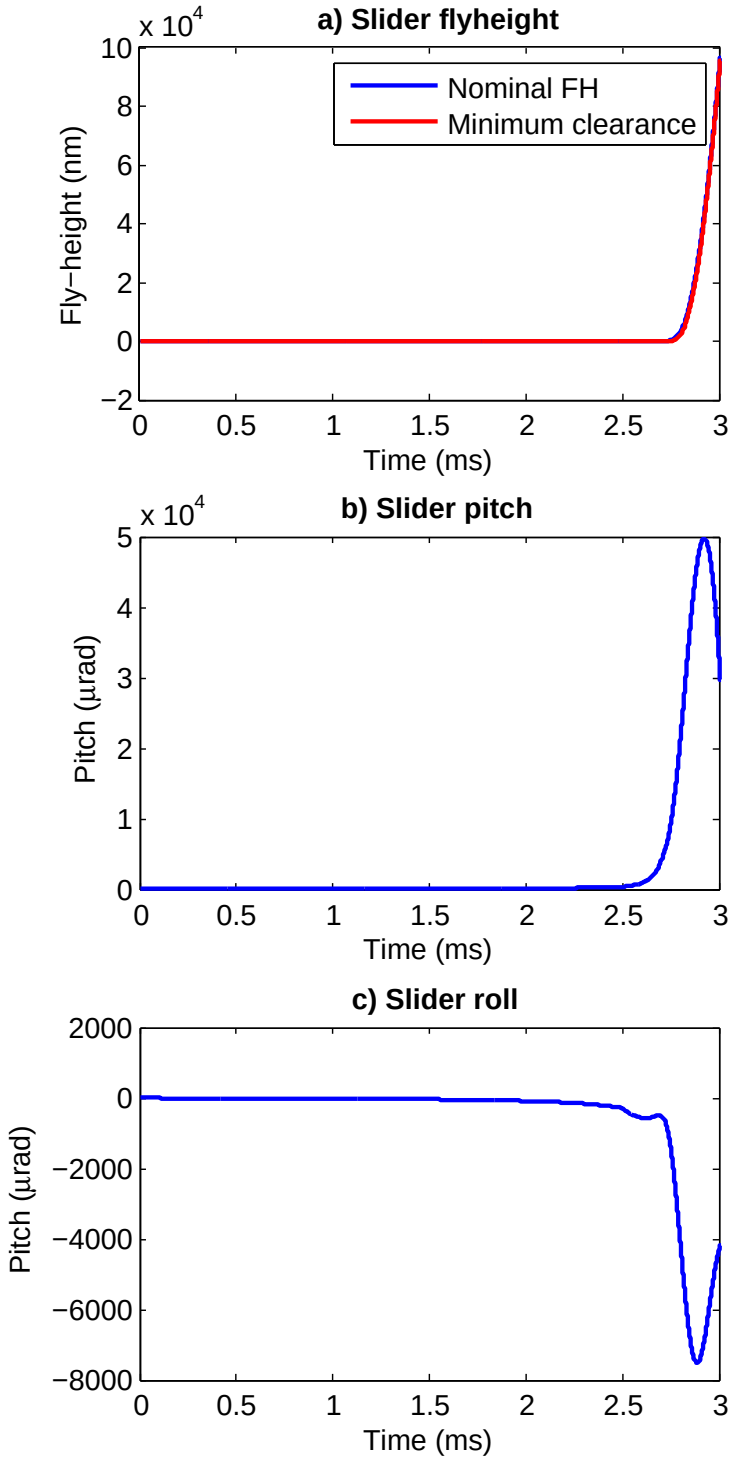

Figure 11: Slider attitude for unloading simulation

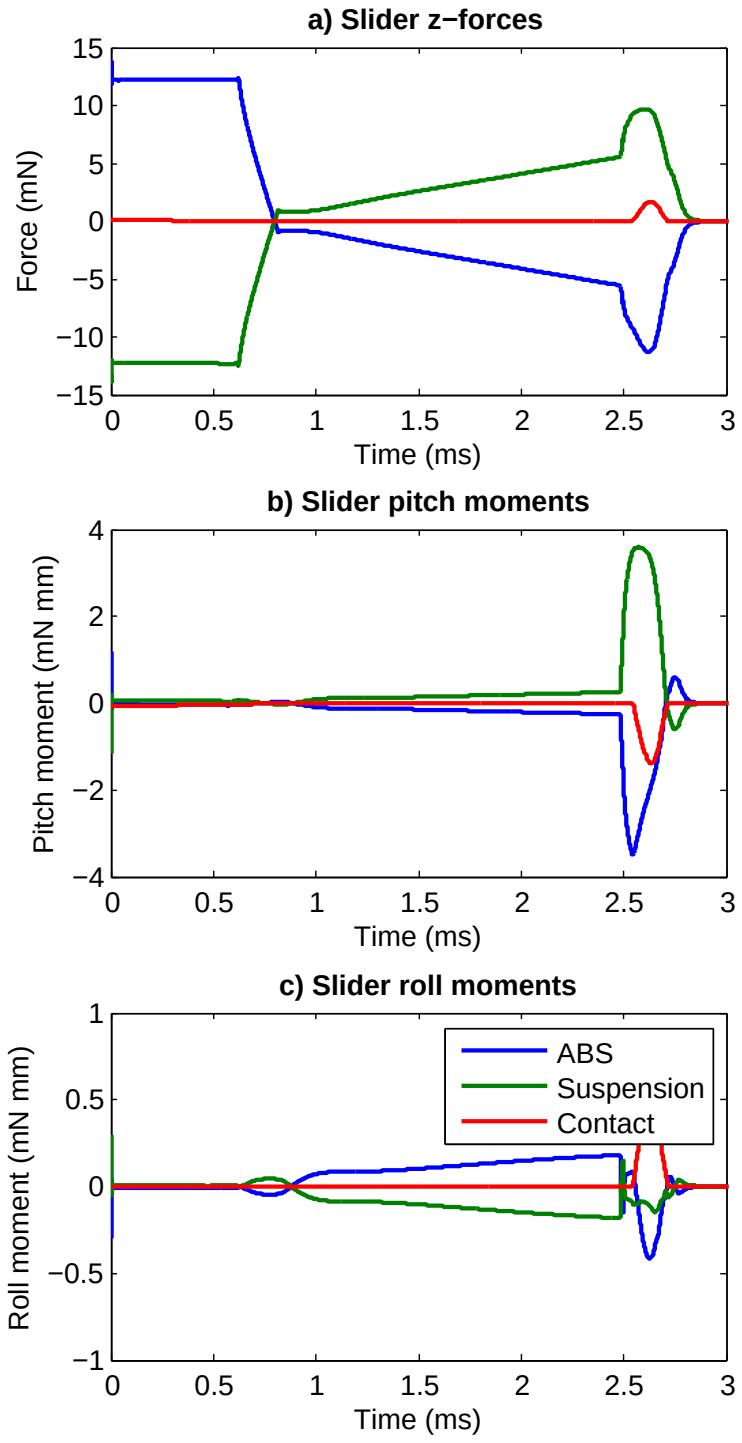

Figure 12: Slider forces for unloading simulation

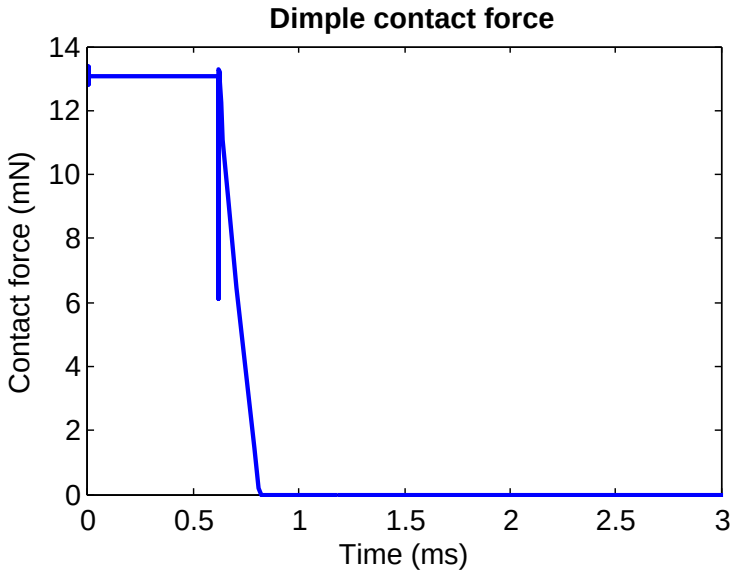

Figure 13: Dimple contact force for unloading simulation

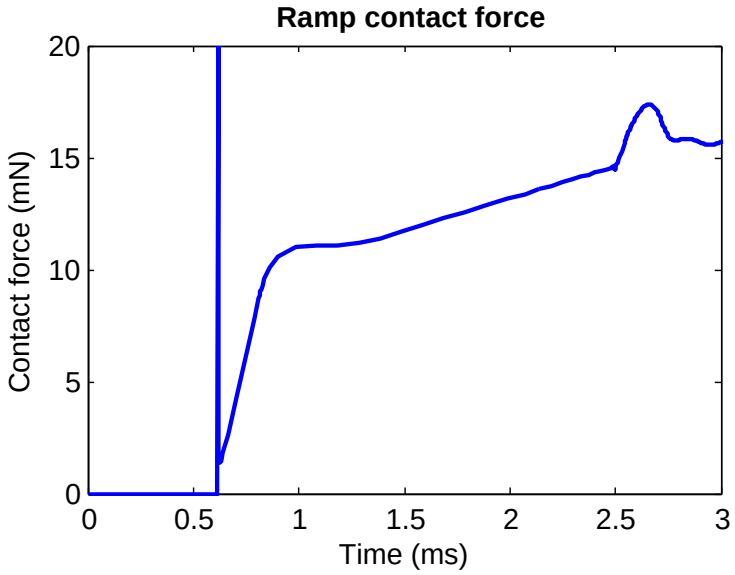

Figure 14: Ramp contact force for unloading simulation

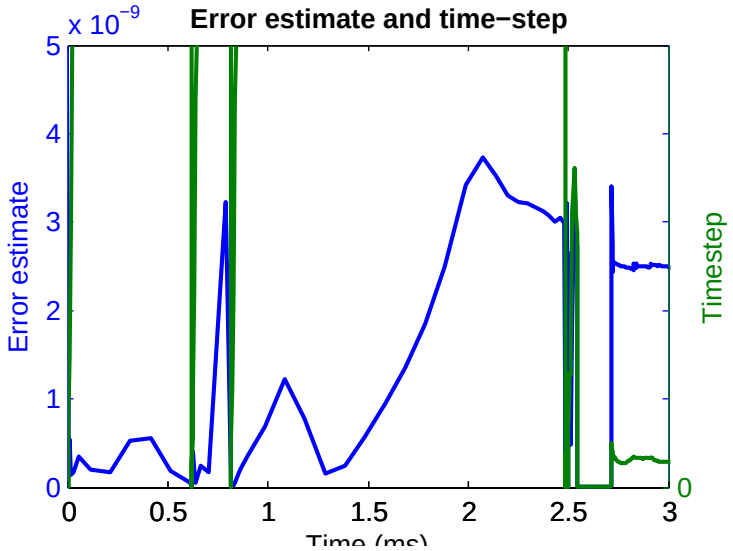

Figure 15: Error-estimate/time-step for unloading simulation